Heavy-ion irradiation effects in the ABO_4 orthosilicates: Decomposition, amorphization, and recrystallization

A. Meldrum, S. J. Zinkle, and L. A. Boatner

Oak Ridge National Laboratory, Oak Ridge, Tennessee 37831-6057

R. C. Ewing

Department of Nuclear Engineering and Radiological Sciences and Department of Geological Sciences, The University of Michigan, Ann Arbor, Michigan 48109-2104

(Received 11 August 1998)

The effects of displacive, heavy-ion irradiation on the properties of synthetic single-crystals of $ZrSiO_4$ (zircon), $HfSiO_4$ (hafnon), tetragonal $ThSiO_4$ (thorite), and monoclinic $ThSiO_4$ (huttonite) have been investigated. All four ABO_4-type orthosilicate materials became amorphous in a process that exhibited a two-stage dependence on temperature when irradiated by 800 keV Kr^+ or Xe^+ ions in the temperature range of 20 to 1100 K. The critical amorphization temperature above which amorphization did not occur increased in the following order: huttonite, zircon, hafnon, thorite. At temperatures below 500 K, the tetragonal and monoclinic polymorphs of $ThSiO_4$ required approximately the same ion fluence for amorphization. Monoclinic $ThSiO_4$ is, therefore, not ''more resistant'' to radiation damage than the tetragonal-symmetry form, but instead, its amorphous phase recrystallizes at a lower temperature. A model that accounts for the observed two-stage behavior was developed and used to calculate the recrystallization activation energies for both stages. When irradiated with heavy ions above a certain characteristic temperature, an unexpected decomposition was observed in which all four ABO_4 orthosilicates phase separated into the crystalline oxides: ZrO_2, HfO_2, or ThO_2 plus amorphous SiO_2. [S0163-1829(99)12205-7]

I. INTRODUCTION

Materials with the ABO_4 composition encompass the structurally, mineralogically, and technologically important orthosilicates including $ZrSiO_4$ (zircon), $HfSiO_4$ (hafnon), and $ThSiO_4$ (tetragonal thorite and monoclinic huttonite) as well as the APO_4 orthophosphates formed by A-site cations of the complete lanthanide transition series. The two common structural forms of these ABO_4-type materials are the tetragonal-symmetry ''zircon'' structure ($I4_1/amd$) and the monoclinic-symmetry ''monazite'' structure ($P2_1/n$). In the tetragonal form, the structure consists of alternating AO_8 (edge-sharing) polyhedra and BO_4 tetrahedra forming chains that are parallel to the fourfold c axis (Fig. 1). The tetragonal and monoclinic structure types are related, and in fact, the lower-symmetry monoclinic form can be derived by introducing a ninth oxygen into the A-site cation-coordination sphere of the zircon structure.[1–3]

In addition to fundamental interest in the response of compositionally similar but structurally different ABO_4 materials to displacive heavy-particle radiation effects, such effects are also of practical interest in a number of technological areas. These areas include the use of $ZrSiO_4$ or $ZrSiO_4$/$HfSiO_4$ mixtures as a host for plutonium resulting from the deactivation of nuclear weapons—an application where the role of radiation effects can be critical;[4–7] the use of natural zircon in geochronology where radiation effects can result in chemical-stability alterations, selective loss of Pb daughter products, and the associated discordant dating of geological formations or accessory minerals;[8–10] and in optical applications involving the use of implantation to form

optical waveguides in $ZrSiO_4$ where radiation damage effects can play a significant role.[11] There are similar as well as additional applications of the structurally related lanthanide orthophosphates,[12–15] and these provided the motivation for our recently reported comprehensive investigations of displacive radiation effects in both the zircon and monazite-
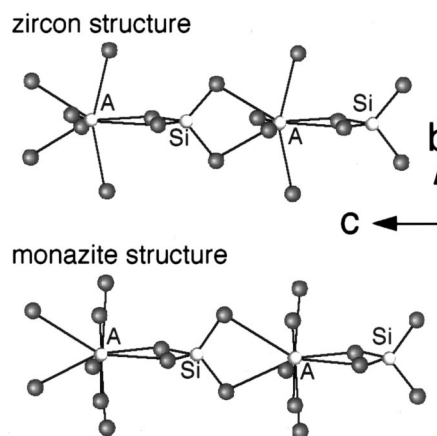

FIG. 1. Ball-and-stick crystal structure diagrams for the ABO_4 orthosilicates $ZrSiO_4$, $HfSiO_4$, and tetragonal $ThSiO_4$ (top), and monoclinic $ThSiO_4$ (bottom), modified after Taylor and Ewing (Ref. 3). In the zircon structure, the A-site cation (Zr, Hf, or Th) is coordinated to eight oxygens (dark spheres), and the structure is composed of cross-linked chains of alternating edge-sharing AO_8 polyhedra and SiO_4 tetrahedra parallel to the c axis. In the monazite structure, a ninth oxygen is introduced into the coordination sphere of the A-site cation resulting in a distortion of the SiO_4 tetrahedra and a lower overall crystal symmetry.

structure rare-earth phosphates.[16] The purpose of the present work is to investigate and directly compare the effects of heavy-ion irradiation on the structural and solid state phase properties of four ABO_4 orthosilicates: $ZrSiO_4$, $HfSiO_4$, and both tetragonal and monoclinic $ThSiO_4$. The present investigations have led to the unanticipated observation of a displacive-radiation-induced phase decomposition of all four ABO_4-type orthosilicates into crystalline AO_2 and amorphous SiO_2 components when irradiated with heavy ions above a certain characteristic temperature.[17]

II. EXPERIMENTAL

Transparent colorless $HfSiO_4$ (diameter=0.5 to 1 mm), $ZrSiO_4$, tetragonal $ThSiO_4$, and monoclinic $ThSiO_4$ (diameter=1 to 5 mm) single crystals were grown by a high-temperature solution process employing a lithium tungstate flux.[18] X-ray diffraction analysis unambiguously confirmed the zircon structure for the synthetic zircon, hafnon, and thorite, and the monazite structure for the huttonite. Some of the crystals exhibited growth habits consisting of subhedral to euhedral square dipyramids, except in the case of monoclinic huttonite, for which the crystal orientations could not be determined by visual inspection. Transmission electron microscope (TEM) specimens of these materials were prepared by hand polishing to a thickness of ~10 μm and then ion-milling using 4 keV Ar^+ ions. Subsequent to perforation of the samples, the Ar^+-ion energy was lowered to 2 keV to minimize surface damage caused by ion milling. Several specimens were also prepared by crushing the crystals in an agate mortar and transferring the resulting powder directly to a carbon-coated copper TEM grid. TEM and energy dispersive x-ray spectrometry (EDS) analyses confirmed that the as-grown crystals contained no crystal-growth flux inclusions or other detectable impurities.

The samples were irradiated by 800 keV Kr^+ ions in the high-voltage electron microscope (HVEM)-Tandem Facility at Argonne National Laboratory. In the case of $ZrSiO_4$, the experiments were repeated using 800 keV Xe^+ ions. Additionally, several of the irradiations were repeated using doubly charged ions. The ion flux varied from 3.4×10^{11} to 3.4×10^{12} $cm^{-2} s^{-1}$ [dose rate=0.0004 to 0.004 displacements per atom (dpa) per second]. The irradiations were performed using a double-tilt He-cooled stage or hot stage allowing a temperature range from 20 to 1100 K to be utilized. Irradiations at 20 K and at 300 K were performed three times for each material in order to estimate the experimental error. Because of possible ionization-induced recrystallization effects arising from electron irradiation,[19,20] the sample was moved out of the electron beam during most of the heavy-ion-irradiation process. In situ electron diffraction was used to monitor the crystalline-to-amorphous (c-a) transition. Subsequent high-resolution imaging was done on a Philips CM200 TEM.

The effect of specimen heating caused by the ion beam was estimated to be minimal under the present experimental conditions by ion irradiating $ZrSiO_4$ crystals at 900 K using several fluxes, ranging from 3.4×10^{11} to 3.4×10^{12} $cm^{-2} s^{-1}$ and then monitoring the temperatures at which amorphization occurred. Additionally, the degree of specimen heating caused by the ion beam was directly quan-

tified by irradiating specimens of the perovskite $KNbO_3$ with 800 keV Kr^+ ions using several ion fluxes. $KNbO_3$ undergoes a ferroelectric phase transition at 690 K, and the temperature at which this transition occurred, as measured at the thermocouple position, was estimated to be approximately 670 K—indicating a maximum temperature increase of ~20 K as a result of the ion-beam heating. Since the thermal conductivities of zircon and the perovskite-structure oxides are roughly similar outside of the cryogenic temperature range, beam heating apparently produces only a minor temperature increase in the orthosilicates for the ion fluxes used in the present study.

The thinnest regions of the specimens usually become amorphous at up to a 50% lower dose than the thicker areas, as discussed in Ref. 21, and accordingly, thickness fringes were used to ensure that the measured fluence for amorphization was obtained from predetermined areas of constant thickness. These were estimated to be roughly 100 nm using extinction distances calculated from the atomic scattering factors for the constituent elements. The fluence required for amorphization of a given specimen was defined by the complete loss of electron-diffraction maxima.

III. RESULTS

A. Low-temperature amorphization

All four orthosilicates were amorphized at relatively low doses by 800 keV Kr^+ ions at temperatures below 300 K (see Fig. 2 and Table I). With increasing fluence, the electron-diffraction maxima were gradually replaced by a diffuse diffraction halo as evident in Figs. 3(a)–3(d). The experimental error, determined by repeating the measurements three times at room temperature and at 20 K, indicated that the maximum variation was ~20% (i.e., for the room temperature irradiation of hafnon) and this maximum value is used in Fig. 2. The ion fluence was converted to an equivalent displacement dose using TRIM-96 calculations (full cascade calculation) with displacement-energy values, E_d, of 79 eV (A-site cation), 23 eV (Si), and 47 eV (O) recently suggested for zircon.[22] Since the E_d values for thorite, huttonite, and hafnon are not established, the known values for zircon were used for these compounds as well.

The critical amorphization dose at 0 K (D_0) was extrapolated from the low-temperature data points, giving average values of 0.16, 0.17, 0.18, and 0.22 dpa for tetragonal $ThSiO_4$, $ZrSiO_4$, monoclinic $ThSiO_4$, and $HfSiO_4$, respectively. Since the maximum experimental variation from the average value obtained for D_0 was approximately 20%, these four values are essentially indistinguishable within experimental error. For all of the materials, the critical amorphization dose (D_c) remained constant up to ~250 K. Between ~250 K and ~350 K the dose increased rapidly, defining a first stage of annealing during irradiation (stage I),[23] before obtaining another plateau value. The actual upper temperature limit of stage I behavior increased from 330 K (Kr^+ irradiation of $ZrSiO_4$) to ~500 K (tetragonal $ThSiO_4$). Stage I annealing was difficult to resolve in the case of tetragonal $ThSiO_4$, possibly due to the experimental error. The observed two-stage behavior is consistent with the previous experimental results reported for $ZrSiO_4$,[23] α-Al_2O_3,[24] $Ca_5(PO_4)_3F$ (apatite),[25] and SiC.[26] The low-temperature data
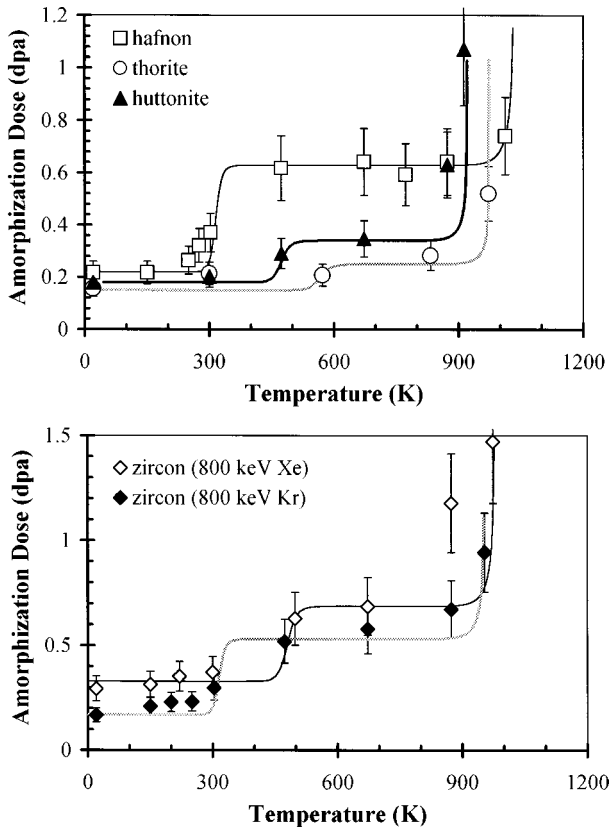
FIG. 2. Critical amorphization dose as a function of temperature for the ABO_4 orthosilicates. The data are divided into two plots for clarity. The 800 keV Kr data are shown for HfSiO$_4$ and the monoclinic and tetragonal ThSiO$_4$ polymorphs (top), and the results for the Kr$^+$ and Xe$^+$ irradiations of ZrSiO$_4$ are shown in the bottom chart. The error bars are 20%, and the lines were obtained by the solution of Eq. (3).

for zircon suggest the possibility of an additional transition at $\sim$150 K (Fig. 2), but additional experimental data are needed to verify the details of the temperature-dose curve in this temperature range.

Varying the dose rate by a factor of 10 and changing the charge state of the ions from +1 to +2 (at a constant ion energy) had no consistent effect on the amorphization dose at room temperature. Specimens prepared by the crushed-grain technique required the same dose for amorphization at room temperature as did the ion-milled samples. These results indicate that the charge state of the ions, the dose rate, and the effects of any amorphous layer produced by ion milling are smaller than the experimental error in determining D_c at room temperature.

B. High-temperature amorphization

Between approximately 400 K and 800 K, the amorphization dose remained constant, but above 800 K it once again increased exponentially (Fig. 2), marking the onset of a second resolvable annealing stage during irradiation. The critical amorphization temperature, T_c, above which amorphization cannot be induced, can be estimated by a visual examination of Fig. 2, or by applying one of several models presently in use to obtain the temperature dependence of the amorphization dose. T_c increased in the following order: monoclinic ThSiO$_4$, ZrSiO$_4$, HfSiO$_4$, tetragonal ThSiO$_4$ (see Table II and Fig. 2). T_c for ZrSiO$_4$ did increase by $\sim$40 K for the Xe$^+$ irradiation. Ion-beam-amorphized monoclinic ThSiO$_4$ was found to recrystallize epitaxially from the thick portions of the specimen at temperatures above 900 K. In contrast, the other orthosilicates did not recrystallize epitaxially after 30 min at the maximum obtainable temperature (1100 K).

C. Irradiation-induced phase decomposition

Although the heavy-ion-induced amorphization of natural zircon has previously been reported at temperatures up to 900 K,[23] in the present study, at temperatures above 900 K for ZrSiO$_4$ and $\sim$950 K for HfSiO$_4$, another effect was observed. Above these transition temperatures (T_t), the irradiated single crystals first became amorphous, and with increasing dose, they decomposed into the component oxides: tetragonal ZrO$_2$ (or HfO$_2$)+amorphous SiO$_2$. At temperatures 150 K above T_t, ZrSiO$_4$ and HfSiO$_4$ decomposed directly into the component oxides (i.e., no intermediate amorphous phase was formed). These observations are documented in the sequences of electron diffraction patterns shown in Fig. 3. T_t is approximately 400 K lower than the temperature at which ZrO$_2$ has been observed to crystallize during thermal annealing of Pu-doped zircon.[27]

A similar radiation-induced decomposition was observed in amorphous ThSiO$_4$ irradiated above 1000 K; however, the reaction was not as abrupt, and the material did not decompose directly to the component oxides at the highest obtainable temperatures (i.e., an intermediate amorphous phase was always formed). Unlike the case for ZrSiO$_4$, the polycrystalline electron-diffraction ring pattern was more intense at certain locations, suggesting the existence of preferred orientations for the ThO$_2$ nanocrystals (see Fig. 4).

The phase decomposition process was more complicated in the case of monoclinic ThSiO$_4$ because of its relatively low critical amorphization temperature. This low T_c leads to competition between ThO$_2$ nucleation and recrystallization

TABLE I. Density (ρ), nuclear cross sections (E_n), electronic and nuclear stopping powers (dE/dx_e and dE/dx_n), critical amorphization fluence (F_0), and amorphization dose at 0 K (D_0) for the orthosilicates.

Compound	ρ g/cm^3	E_n eV cm^2/10^{15} atoms	dE/dx_n eV/A	dE/dx_e eV/A	F_0 ×10^{14} cm^{-2}	D_0 dpa
zircon	4.61	1.83	138	127	1.48	0.17
zircon (Xe)	4.61	2.45	292	120	1.28	0.33
hafnon	6.97	1.92	155	128	1.50	0.22
huttonite	7.18	2.04	136	123	1.21	0.18
thorite	6.69	2.04	127	115	1.15	0.16

TABLE II. Activation energies and critical amorphization temperatures calculated using the Weber *et al.* model (stage II only: Ref. 23) and Eq. (3). Application of Eq. (3) to calculate these values requires high-dose amorphization data, i.e., points high up along the curves in Fig. 2. Such high-dose data are generally lacking in the orthosilicates because the materials are amorphized at relatively low doses below the phase-decomposition temperatures. This is particularly true in the case of thorite; hence, the tabulated E_a and T_c values may be slightly low.

| Compound | Weber *et al.* model (Ref. 23) | | Equation (4) | | |
	E_a (eV)	T_c (K)	E_{cp} (eV)	E_a (eV)	T_c (K)
zircon	0.37	1132	1.0	3.3	1000
zircon (Xe)	0.003	1615	1.5	3.4	1040
hafnon	1.04	1193	1.0	3.5	1070
huttonite	0.29	990	1.5	3.1	950
thorite	0.31	1107	1.8	>3.6	>1100

of huttonite. An additional unexpected observation was made in the case of monoclinic $ThSiO_4$ irradiated at high temperature: i.e., a network of circular ''islands'' with dark contrast appeared within a matrix consisting of distorted huttonite and randomly oriented ThO_2 (see Fig. 5). These features are approximately 20 nm in diameter and are either single crystals or a collection of randomly oriented nanocrystals. In some cases, Moiré fringes arise because of interference with the host matrix [Fig. 5(b)]. High-resolution imaging of these structures routinely gave lattice fringes with a 3.1 ± 0.2 Å spacing, consistent with the (111) lattice spacing of cubic ThO_2 (3.06 Å). Focused-probe EDS analysis confirmed that these grains were indeed Si deficient. The diffraction patterns in Figs. 4 and 5 show that all orientations of ThO_2 are present but there is some texturing that appears to favor certain directions. The oxide nanocrystals were, however, not oriented with respect to the original matrix.

A series of irradiations was performed near the characteristic phase-decomposition temperatures to investigate the kinetics of this irradiation-induced reaction in $ZrSiO_4$ and $HfSiO_4$. The $ThSiO_4$ compounds were not similarly investi-

gated because of the high temperatures required for the reaction to occur. The relative rates of the crystalline-to-amorphous-to-polycrystalline (c-a-p) transitions as a function of temperature are shown in Fig. 6. High-resolution microscopy confirmed the presence of nanocrystalline ZrO_2 in $ZrSiO_4$ and HfO_2 in $HfSiO_4$ irradiated above 900 K and 950 K, respectively (Fig. 7). Broad-beam and focused-probe EDS techniques confirmed the presence of SiO_2.

Ion-beam amorphized samples of $ZrSiO_4$ and $HfSiO_4$ were heated to 1100 K and held for 30 min to determine if the phase decomposition was due to thermal annealing. No crystallization of ZrO_2 or HfO_2 was observed in the amorphous samples. However, when the ion beam was allowed to impinge on an amorphous specimen at this temperature, the oxides rapidly precipitated from the amorphous matrix. The component oxide phases did not subsequently redissolve into the matrix when held for 30 min at 1100 K.

D. Thermal annealing

Ion-beam-amorphized specimens of all four orthosilicates were heated between 1000 and 1100 K and held at these
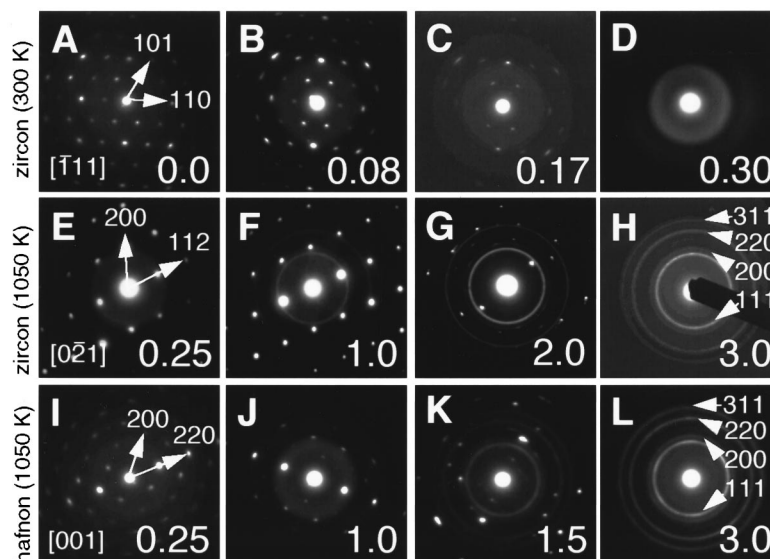

FIG. 3. Sequences of electron-diffraction patterns documenting the effects of ion irradiation at different temperatures. The dose in dpa is given at the bottom right of each diffraction pattern and the arrows point to higher-order spots for clarity. The polycrystalline rings in H and L are indexed to tetragonal ZrO_2 and HfO_2, respectively.
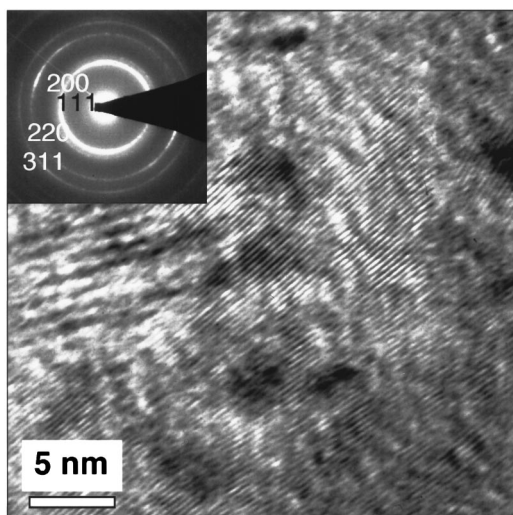
FIG. 4. High-resolution TEM image of tetragonal $ThSiO_4$ irradiated at 1100 K to a dose of 2.5 dpa. The corresponding electron-diffraction pattern is shown in the inset. The material is comprised entirely of weakly textured cubic ThO_2. Moiré-fringe contrast at the left of the image arises from the superposition of two or more ThO_2 ''nanocrystals.''

FIG. 6. Relative rates of the c-a-p transitions in $ZrSiO_4$ and $HfSiO_4$. Transitions labeled ''fast'' are arbitrarily defined as occurring after less than 2 min of irradiation, and ''slow'' indicates longer than 5 min at an ion flux of 1.7×10^{12} cm^{-2} s^{-1}.

temperatures for 1 to 30 min. For $ZrSiO_4$, $HfSiO_4$, and tetragonal $ThSiO_4$, no crystallization (epitaxial or spontaneous nucleation) was observed. In the case of monoclinic $ThSiO_4$, however, the heated samples gradually recrystallized epitaxially from the thicker portions of the TEM specimen which were not fully penetrated by the ion beam. Crystallization was not observed after 30 min at temperatures below 900 K, but at 1000 K the material completely recrystallized within 5 min. The resulting material was mostly single-crystal huttonite. In some areas of the specimen, huttonite crystals nucleated with new orientations (Fig. 8).

There are numerous reported studies of fission-track annealing in zircon (e.g., Refs. 28–30). There are, however, no reported epitaxial recrystallization studies for $HfSiO_4$ or either polymorph of $ThSiO_4$. The temperatures at which epitaxial thermal annealing of monoclinic $ThSiO_4$ was observed ($T > 900$ K) are lower than the experimentally determined thorite-huttonite transition temperature of ~ 1250 K.[31] The

present results demonstrate that recrystallization of monoclinic $ThSiO_4$ is possible at a temperature lower than that required for nucleation from a bulk amorphous material and that recrystallization can, in fact, occur in the stability field of tetragonal $ThSiO_4$. On the other hand, ion-beam-amorphized tetragonal $ThSiO_4$ exhibited no inclination to recrystallize when held at 1100 K for 30 min.

The observation that huttonite is ''invariably crystalline'' in nature[3,32] has lead to the conclusion that the monoclinic huttonite polymorph of $ThSiO_4$ is ''more resistant'' to radiation damage than tetragonal thorite.[3] This conclusion is not consistent with the data presented here. The amorphization dose is similar for these two compounds over a wide range of temperature (Fig. 2), and the critical amorphization temperature for huttonite is relatively high (~ 950 K) when compared with some other orthophosphates and orthosilicates [e.g., monazite ($CePO_4$): 440 K;[33] phosphate and silicate apatite: 475 and 711 K, respectively;[34] and forsterite (Mg_2SiO_4): 480 K (Ref. 35)]. This observation suggests that huttonite should become metamict in natural samples. Monoclinic $ThSiO_4$ is, however, clearly more susceptible to epitaxial thermal recrystallization than the zircon-structure orthosilicates, and over geologic time scales, it is possible that long-term thermal annealing processes may overcome the effect of self-radiation damage. In other words, the relative amount of radiation damage caused by heavy-ion irradiation is approximately the same in monoclinic and tetragonal $ThSiO_4$, but the damage is more readily annealed in the monoclinic structure.
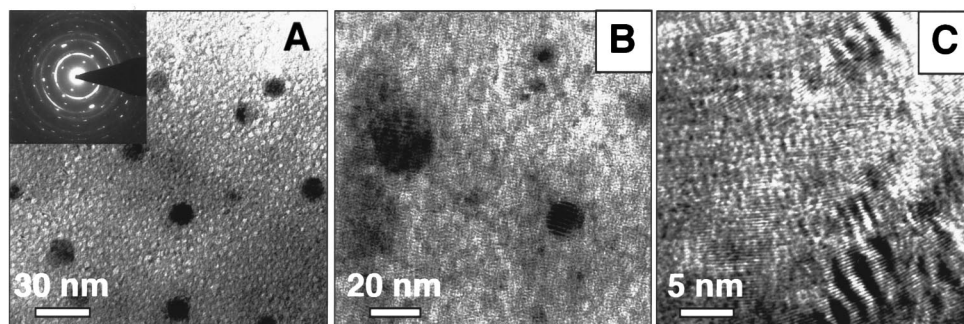

FIG. 5. Bright-field TEM images of monoclinic $ThSiO_4$ irradiated at 900 K to a dose of 1.5 dpa. The electron-diffraction pattern shows diffraction maxima from the huttonite matrix and the characteristic polycrystalline rings from ThO_2. In (A), the ThO_2 is visible as a fine-grained mottled texture. Isolated ''islands'' with an average diameter of approximately 20 nm are visible in (A) and (B). These were found to be either single crystals, as indicated by the Moiré fringes in (B), or to be composed of aggregates of misoriented crystallites. Panel (C) shows ThO_2 crystallites, highlighted by the Moiré fringe contrast, in a matrix of distorted huttonite.
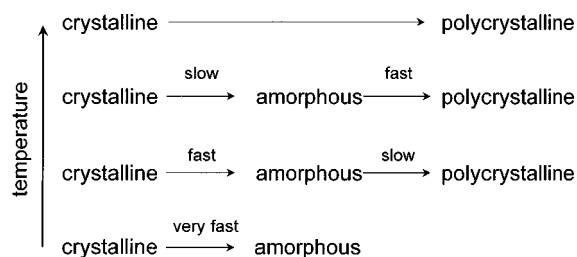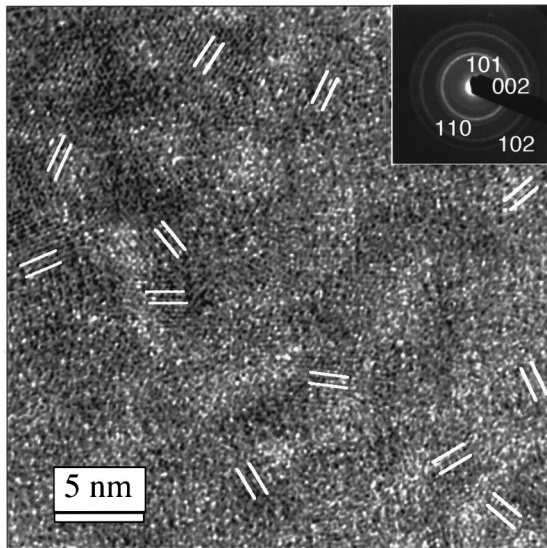
FIG. 7. High-resolution TEM micrograph of $ZrSiO_4$ irradiated to a dose of 3 dpa at 1050 K, showing randomly oriented ZrO_2 nanocrystals in an amorphous SiO_2 matrix. There is no preferred orientation of the ZrO_2 nanocrystals.

E. Amorphization-resistant crystalline regions

Small isolated regions (so-called radiation-resistant experimental ''outliers'') of most specimens remained crystalline at doses that were several times higher than those required to amorphize the majority of the sample. This phenomenon has previously been observed in single-crystal samples studied using the methods employed here. It has been discussed in some detail by Smith et al.,[36] and the possible explanations advanced were (i) electron-beam annealing, (ii) shadowing of the ion beam by the specimen holder, (iii) annealing at elevated temperatures caused by ion-beam heating due to locally poor thermal contact between the specimen and the copper support grid, (iv) ion channeling, or (v) local compositional differences. Electron-beam irradiation was determined not to be a factor in the present experiments, shadowing was not an issue since the irradiated regions were in the center of the specimens, and the synthetic samples contained no major impurities—indicating that local compositional differences are not the cause of these small anomalous regions. The degree of ion-beam heating that would be required to explain these regions, in $ZrSiO_4$ for
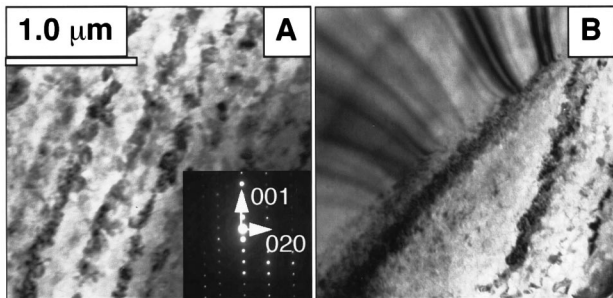

FIG. 8. Ion-beam-amorphized monoclinic $ThSiO_4$ annealed at 1100 K for 10 min. Most of the material crystallized epitaxially from the thick portions of the TEM specimen as in (A); however, in some locations new orientations were nucleated (B).

example, would have to be ~700 K, while the temperature calibration using the phase transition of $KNbO_3$, as noted above, indicated beam-heating effects on the order of 20 K. In any event, the amorphization doses obtained for these anomalous regions were not analyzed or included in the results presented here.

IV. DISCUSSION AND ANALYSIS

A. Amorphization kinetics

Several models describing radiation-induced amorphization and crystallization in non-metals have previously been developed[37–39] including the model of Weber et al.,[23,25] in which the effect of increasing temperature is assumed only to decrease the amount of damaged material produced within each displacement cascade (i.e., thermal annealing of the damaged region after the displacement cascade has quenched is ignored). Molecular dynamics calculations performed on metals have found that the damage rate is only weakly affected by temperature[40] and that most of the experimentally observed decrease in residual damage with increasing temperature is due to post-cascade lattice annealing. Therefore, the fundamental assumption of the Weber et al.[23] annealing model seems questionable. A reasonable fit to the experimental data can generally be obtained, but the calculated activation energies are unrealistically low [these are typically in the range of 0.1 eV for processes that occur near or above 500 K (e.g., Ref. 34) and, in some cases, values as low as 0.009 eV have been reported[25]]. Additionally, where two or more annealing stages are defined, as in the present work, each of these stages must be modeled separately.

An alternative amorphization model can be derived if thermal annealing is considered to be a continuous process[41] (i.e., annealing does not ''stop'' after the thermal spike phase of the collision cascade). For simplicity, the derivation which follows assumes that amorphization occurs directly in the displacement cascades and that the annealing of amorphous regions occurs with two discrete activation energies (stage I and stage II annealing). The process of amorphization via multiple overlapping cascades and recovery with more than two activation energies can be obtained from an extension of this simple model. The two activation energies may be associated with low-temperature close-pair recombination and high-temperature epitaxial recrystallization, respectively.[23] According to this approach, damaged regions (e.g., at the edges of the cascade) may recover by close-pair recombination at a temperature of 300 K in zircon irradiated with 800 keV Kr^+ ions—leading to an increase in the amorphization dose over this range of temperatures. At higher temperatures, all close pairs may have recombined and the amorphization dose becomes constant (stage II annealing). Stage I could alternatively be associated with other types of defects; however, the mathematical form of the following derivation is not affected. The following simple kinetic equations (see Appendix A for details) can then be formulated to describe the production and thermal annealing of amorphous zones:

$$\frac{df_a}{dt} = P[1 - \varepsilon(1 - ^{-\lambda_{cp}t})](1 - f_a) - \lambda_a f_a, \quad (1)$$

$$\lambda = Ae^{-E_i/kT} = \nu \cdot e^{[\Delta S_i/k - H_i/kT]}, \quad (2)$$

where f_a is the atomic fraction of atoms which are contained in the amorphous phase, P is the production rate of amorphous zones directly in the displacement cascade (in units of dpa/s), ε is related to the fraction of metastable disordered atoms in the cascade that experience correlated (intracascade) close-pair recombination during stage I annealing [$\varepsilon = (D_{0(\text{stage II})} - D_{0(\text{stage I})})/D_{0(\text{stage II})}$], and λ_{cp} and λ_a are rate constants for close-pair recombination and recrystallization of isolated amorphous zones at temperature T. In Eq. (2), ν is the lattice vibration frequency ($\sim 10^{13}$ Hz), k is Boltzmann's constant, t is the irradiation time to produce a given amorphous fraction, and ΔS_i and E_i are the entropy change and activation enthalpy associated with the amorphous-to-crystalline transformation (i is replaced by cp or a for close-pair recombination and recrystallization of amorphous zones, respectively). The solution to Eq. (1); using the initial condition that $f_a = 0$ at $t = 0$, is given by

$$f_a = \frac{P}{P+\lambda'}[1 - e^{-(P+\lambda')[(1-\varepsilon)t+(\varepsilon/\lambda_{cp})(1-e^{-\lambda_{cp}t})]}], \quad (3)$$

where $\lambda' = \lambda/(1-\varepsilon)$ and t is the irradiation time to produce a given amorphous atom fraction at temperatures well above the close-pair recombination temperature regime. In order to obtain an analytic solution for the differential equation (1), the simplifying approximation was made that $P + \lambda_a/(1-\varepsilon + \varepsilon e^{-\lambda cpt}) \sim P + \lambda_a/(1-\varepsilon)$ (see Appendix A). Equation (3) is transcendental with respect to t, so the solution must either be obtained by iteration or a simplifying assumption made with respect to t. Equation (3) can be rearranged in a simplified form:

$$t = \frac{A-B}{C(1-\varepsilon)}, \quad (4)$$

where A is the contribution from isolated amorphous zones

$$A = -\frac{\ln\left[1 - \frac{f_a(P+\lambda'_a)}{P}\right]}{P+\lambda'_a} \quad (5)$$

and B represents the contribution from close pairs

$$B = \frac{\varepsilon(1-e^{-\lambda_{cp}t})}{\lambda_{cp}}. \quad (6)$$

B is dependent on t, reflecting the transcendental nature of Eq. (3). The factor C relates the total number of disordered and displaced atoms (Pt) to the Kinchin-Pease[42] dpa value:

$$C = \frac{Pt}{D_c}. \quad (7)$$

The damage production rate, P, can be significantly greater than the Kinchin-Pease displacement rate since the unit ''dpa'' does not include disordered lattice defects. Atomic disordering may produce a total defect concentration (displaced plus disordered atoms) that is considerably higher than the Kinchin-Pease displacements per atom. For example, an amorphous fraction of $f_a = 0.95$ is attained at low temperature for a ''disordered'' damage level of $Pt = 3$, whereas ''complete'' amorphization[43] ($f_a \geq 0.95$) occurred

in the orthosilicates in the present study at a dose of ~ 0.2 dpa at 20 K. This suggests that the disordering (amorphization) rate for 800 keV Kr^+ ions is approximately an order of magnitude higher than the dpa rate ($C \sim 15$). It is interesting to note that an earlier curve-fitting analysis for amorphization of Pu-doped zircon[23] obtained a damage scaling parameter of $C = 9.5$/dpa, although the authors did not comment on the significance of a damage rate that was an order of magnitude higher than the Kinchin-Pease dpa rate.

The critical amorphization dose in terms of dpa is found by multiplying the irradiation time from Eq. (4) by the dose rate: $D_c = Pt/C$. The critical temperature at which amorphization cannot proceed (T_c) is found by setting the right-hand side of Eq. (1) equal to zero. If it is assumed that close-pair recovery occurs at temperatures much lower than T_c (i.e., $\exp(\lambda_{cp}t) \sim 0$ at $T = T_c$), then the resultant expression is

$$T_C = \frac{E_a}{k\ln\left[\dfrac{Af_a}{P(1-\varepsilon)(1-f_a)}\right]}. \quad (8)$$

Equations (3)–(8) may also be derived without the simplifying assumptions. For example, the slope of the calculated lines in Fig. 2 can be modified by assuming that the annealing of amorphous zones occurs through a multi-activation-energy process. P, the damage production rate, can be modified to model amorphization via the overlap of two or more displacement cascades. The assumptions used in the derivation of Eq. (3), however, do not appreciably change calculated activation energies.

Using Eq. (3), the activation energies for stage II annealing in the orthosilicates range from 3.1 to ~ 3.6 eV. These values were obtained by requiring the curve to pass through the highest-dose data point. Thus, the calculated E_a and T_c values will be most accurate for those compounds for which high-dose data are available. Even at the highest temperatures obtainable in the electron microscope, the amorphization dose for the orthosilicates (especially tetragonal $ThSiO_4$) is relatively low and the calculated activation energy may, therefore, be low by several tenths of an electron volt. The activation energy for stage I annealing was calculated to be 1.0–1.8 eV for the orthosilicates (Table II). The amorphization dose at room temperature was independent of flux between 3.4×10^{11} and 3.4×10^{12} cm^{-2} s^{-1} (within experimental error), suggesting that at least the stage I activation energies correspond to first-order reaction kinetics. A close examination of the low-temperature data in Fig. 2 suggests that, for $ZrSiO_4$ at least, there may be more than one low-temperature close-pair annealing stage (there is a relatively large jump in D_c between 100 and 200 K). Equation (1) is flexible in that another close-pair annealing term could be added to model additional recombination mechanisms.

The physical meaning of the activation energies obtained from Eq. (3) are difficult to ascertain; however, the magnitudes of E_{cp} and E_a may be characteristic of certain types of processes. For example, E_{cp} varies from approximately 1 to 1.8 eV. These values can be compared to the known defect migration energies in other insulating ceramics, as summarized in Ref. 44. In general, the present values obtained for the orthosilicates are similar to interstitial migration energies

in Al_2O_3 and MgO, but are slightly lower than the activation energies for vacancy migration (these vary from 1.8 to 2.5 eV). On the other hand, the values obtained for E_a (3.1 to ~3.6 eV) are quite high. These could be associated with vacancy migration or, more likely, epitaxial recrystallization of amorphous zones. This latter hypothesis is supported to some degree by the value of 3.6 eV recently obtained for the recrystallization of fission tracks parallel to the c axis in natural zircon.[28]

At 20 K, the amorphization dose was the same for the orthosilicates within experimental error, subject to the assumed displacement energies for $HfSiO_4$ and the two polymorphs of $ThSiO_4$. Consequently, the commonly used indicators for the susceptibility to amorphization, such as average bond ionicities,[45] Gibbs free energy,[46] bond distortions,[46] structural connectivity,[47] or combinations of these parameters[48,49] do not correlate with the amorphization doses at 20 K, or with the observed sequence of T_c values. Hobbs' structural-connectivity model[47] predicts that the huttonite structure should be more resistant to amorphization at 0 K; however, this predicted difference was not experimentally resolvable in the present study.

The amorphization dose at room temperature generally does not follow the same ranking as the critical amorphization temperatures. These differences are caused by the kinetics of annealing at elevated temperatures, and models which ''rank'' amorphization resistance must include kinetic considerations. Thus, Hobbs' model[47] will be most accurate at temperatures at which there is no kinetic contribution to the annealing process (i.e., in the low-temperature straight-line portions of the curves in Fig. 2). Wang's semiempirical model[48] indirectly includes kinetic considerations by comparing solid-state amorphization to glass formation, with the assumption that defect mobility under ion irradiation scales with viscous flow in glasses. The main point of the present observations is that kinetic factors can have a significant effect on the amorphization behavior.

B. Irradiation-induced phase decomposition

The present experiments clearly demonstrate that the phase decomposition discovered at elevated temperatures (e.g., $ZrSiO_{4(c)} \rightarrow ZrO_{2(c)} + SiO_{2(a)}$) is caused directly by the heavy-ion irradiation. Much of the prior work involving the nucleation of new phases under heavy-ion irradiation was done on metallic alloys for fission reactor applications (e.g., Ref. 50). The nucleation of these phases occurred largely as a result of enhanced diffusion and solute segregation due to the high concentrations of radiation-induced point defects in the crystalline solid. In the case of nonmetals, Newcomer et al.[51] observed thallous oxide (Tl_2O) to form as a result of ion irradiation of a Tl-Ba-Ca-Cu-O superconductor. Wang et al.[52] reported the nucleation of magnetite (Fe_3O_4) and crystalline quartz (SiO_2) from ion-beam-amorphized γ-$SiFe_2O_4$ at 873 K. Crystalline quartz will normally amorphize under these irradiation conditions,[48] and the mechanism by which the SiO_2 apparently crystallizes under these same conditions (but in a different host) is not known. These are the only known previous examples of nonmetals in which phases were observed to nucleate in an amorphous matrix as a result of ion irradiation.

The temperature required to induce the phase decomposition increased in the order $ZrSiO_4$, $HfSiO_4$, tetragonal $ThSiO_4$. $ZrSiO_4$ and $HfSiO_4$ decomposed directly into the component oxides at 1100 K (i.e., no amorphous phase was formed). Tetragonal $ThSiO_4$ could be amorphized at 1100 K (it did not decompose directly, as did zircon and hafnon), but polycrystalline rings corresponding to ThO_2 subsequently developed at high doses ($\sim 5D_c$). Thus, these transitions are shifted to higher temperature in the case of tetragonal $ThSiO_4$. The phase decomposition could not be completed in monoclinic $ThSiO_4$ because the material recrystallized epitaxially at 1000 K.

A possible explanation for the presence of crystalline precipitates at high temperatures (but below T_c) in the displacement cascades of irradiated zircon and hafnon and their near absence in thorite can be made based on the thermal spike model. The thermal-spike mechanism has been extensively debated in the literature,[53,54] and the existence of the thermal-spike phase of collision cascades in insulating ceramics remains open to question although the model has strong support from molecular dynamics simulations in metals.[55–57] While the studies on metals provide some evidence for the formation of a liquid-like state inside the displacement cascades, such behavior has not been demonstrated in the case of insulating ceramics.

In the present investigations of the ABO_4 orthosilicates, heavy ion irradiation produces a decomposition and phase segregation of the material into an AO_2 crystalline oxide and amorphous SiO_2. Since a similar situation results from the melting and resolidifying of $ZrSiO_4$, the present results are not inconsistent with the presence of a ''liquidlike'' state within the cascade. An examination of the published ZrO_2-SiO_2 phase diagram[58] shows that a crystalline ZrO_2 phase coexists with an SiO_2-rich liquid phase at temperatures between 1960 and 2675 K for a composition of $ZrSiO_4$. Relatively rapid liquid-phase diffusion can occur in this temperature range. A solid solution of crystalline SiO_2 and ZrO_2 occurs below the eutectic solidus temperature of 1960 K (with correspondingly slower solid-state diffusion parameters), and the solid-state (peritectoid) reaction $ZrO_2 + SiO_2 \rightarrow ZrSiO_4$ occurs at 1949 K. Based on the estimated average kinetic energy for the ~1000 atoms contained within the individual displacement cascade regions, the effective temperature should exceed the melting point for zircon. According to the thermal spike model, the relatively high quench rate through the two-phase region (crystalline ZrO_2 and SiO_2-rich liquid), which occurs for low ambient temperatures, would not allow sufficient time for nucleation of the crystalline ZrO_2 phase. However, decreasing the cooling rate at temperatures in the two-phase region between 2670 and 1960 K by increasing the ambient temperature could allow the nucleation of tetragonal ZrO_2 in the displacement cascade region.

The HfO_2-SiO_2 phase diagram[59] shows a two-phase region (tetragonal HfO_2 plus SiO_2-rich liquid) from 2875 to 2025 K for a composition of $HfSiO_4$. A peritectic reaction to form hafnon occurs at 2025 K. The higher peritectic solidus temperature in hafnon as compared with the eutectic solidus temperature in zircon roughly coincides with the difference in minimum temperatures for the formation of crystalline
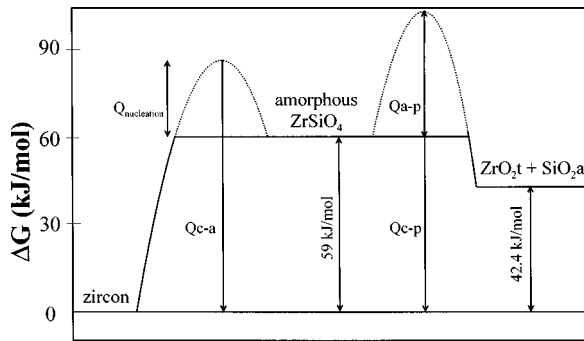
FIG. 9. Free energy diagram for $ZrSiO_4$ derived from the present results and from those in Ref. 64. The relative ''heights'' of the Q_{c-a} and Q_{a-p} energy barriers are inferred from the irradiation results, but the absolute magnitudes are not known (hence the dotted lines).

HfO_2 vs ZrO_2 crystallites in the displacement cascades of the two materials (950 vs 900 K). The $ThSiO_4$ phase diagram[60] shows a two-phase region (crystalline ThO_2 plus SiO_2-rich liquid) from ~2475 to 2250 K for a composition of $ThSiO_4$, and thorite is formed by a peritectic reaction with a solidus temperature of 2250 K. The relatively small temperature range between the liquidus and the solidus (and also the relatively high solidus temperature for thorite as compared with hafnon and zircon) is not favorable for the precipitation of ThO_2, therefore, precipitation of ThO_2 from some ''liquid-like'' state in a displacement cascade would require higher ambient temperatures, and the transformation to the component oxides occurs less readily than for the cases of zircon and hafnon.

In the thermal spike model, the temperature within the cascade region is characterized by a characteristic cooling rate $\exp(-t/\tau)$, where t is time, and τ for metals such as nickel with strong electron-phonon coupling is ~1 ps.[61,62] If we approximate the thermal conductivity of the orthosilicates at $T > 1800$ K as being an order of magnitude lower than the thermal conductivity of Ni, the cooling time constant for the orthosilicates should be $\tau \approx 10$ ps. The magnitude of the diffusion coefficient necessary to produce solute segregation within the displacement cascade region can be estimated to be $D \approx x^2/t = 1 \times 10^{-8}$ m^2/s where $x = 1.5$ nm is the observed crystallite radius for ZrO_2 (comparable to cascade dimensions) and $t \approx 3\tau = 30$ ps is the thermal-spike lifetime. This estimate is similar to known liquid diffusion coefficients.[63]

C. Thermodynamic considerations

On the basis of the present observations and earlier results,[64] a free-energy diagram can be constructed for the orthosilicates (Fig. 9). Entropy contributions to the free energy are not considered, and these are generally small in comparison with the enthalpy changes.[65] The transformation from crystalline-to-amorphous zircon requires an energy input of 59 kJ/mole.[64] Amorphous $ZrSiO_4$ does not spontaneously recrystallize, even over a geologic time scale, so the presence of a crystal nucleation barrier Q_{c-a} is inferred. The absolute magnitude of Q_{c-a} is not known; however, these results show that Q_{c-a} is less than Q_{a-p} (the energy barrier for the transformation from the amorphous phase to the component oxides).

At low irradiation temperatures, the free energy of the damaged, defect-rich substrate increases until the energy barrier Q_{c-a} is overcome and the material ''relaxes'' into the amorphous state (Q_{c-a} corresponds to the free energy of a defect-rich crystalline phase). A good approximation for Q_{c-a} may be the latent heat of melting. At higher temperatures, the same c-a transformation occurs, but the energy barrier Q_{a-p} can now also be overcome and ZrO_2 may nucleate in the amorphous matrix. At the highest irradiation temperatures, both Q_{c-a} and Q_{a-p} are simultaneously overcome (no relaxation into the amorphous phase), and the direct transformation $ZrSiO_{4(c)} \rightarrow ZrO_{2(c)} + SiO_{2(a)}$ can occur.

The preceding analysis does not account for the kinetics of the c-a-p transformations and the application of equilibrium phase diagrams is clearly only an approximation to the actual situation inside a highly nonequilibrium displacement cascade. Additionally, if the thermal conductivity of amorphous zircon is lower than for the crystalline material (as for many other amorphous ceramics), then the quench rate decreases with increasing damage. This would enhance the amorphous-to-polycrystalline transformation to the component oxides at moderate temperatures.

V. SUMMARY AND CONCLUSIONS

Synthetic $ZrSiO_4$, $HfSiO_4$, and monoclinic and tetragonal $ThSiO_4$ single crystals were irradiated by 800 keV Kr^+ ions. The crystalline-to-amorphous transition was investigated as a function of temperature from 20 to 1100 K and the following observations were made.

The critical amorphization doses for the orthosilicates were found to increase in at least two major stages with transitions occurring at approximately 300 for $ZrSiO_4$ and $HfSiO_4$, and ~550 K for tetragonal $ThSiO_4$.

The extrapolated critical amorphization temperatures increase in the order monoclinic $ThSiO_4$, $ZrSiO_4$, $HfSiO_4$, tetragonal $ThSiO_4$.

At elevated temperatures, the D_c-vs-temperature curves for $ZrSiO_4$ and $HfSiO_4$ were interrupted and the materials decomposed into the component oxides, i.e, tetragonal ZrO_2 or HfO_2 + amorphous SiO_2. Tetragonal $ThSiO_4$ required higher temperatures to induce the same decomposition to the component oxides.

Monoclinic $ThSiO_4$ could be thermally recrystallized at relatively low temperatures (~1000 K). This relatively low recrystallization temperature may explain the lack of observed α-decay-induced metamictization in natural huttonite.

A model was developed and used to calculate the activation energies for the two annealing stages. Stage I is tentatively ascribed to close pair recombination, and the calculated E_{cp} values are close to the interstitial migration energies for other insulating ceramics. Stage II is probably related to the annealing of amorphous zones, and the E_a values are in the range of 3.1 to 3.6 eV for processes which occur at temperatures in excess of 1000 K. If the phase decomposition observed at elevated temperatures is associated with the creation of a liquidlike state in the collision cascade, then the liquid diffusion coefficient inside the cascades is estimated to be approximately 10^{-8} m^2/s.

APPENDIX

The production of amorphous regions during ion irradiation is assumed to consist of two components: well-developed damaged (amorphous) zones which are produced in the central region of displacement cascades, and isolated point-defect disorder which is produced near the periphery of the cascade. The isolated point-defect damage is assumed to anneal with a lower activation energy compared to the clustered damage produced in the core of the cascade.

The following coupled differential equation describes the production and annealing of the close-pair (f_{cp}) and displacement cascade (f_a) defect fractions:

$$\frac{df_a}{dt} = (1-\varepsilon)P(1-f_a) + \frac{df_{cp}}{dt} - \lambda f_a, \qquad (A1)$$

$$\frac{df_{cp}}{dt} = P\varepsilon(1-f_a) - \lambda_{cp}f_{cp}. \qquad (A2)$$

The linear homogeneous differential equation (A2) can be solved by standard methods with the simplifying assumption that f_a is constant. This assumption is discussed below. Using the boundary condition $f_{cp}=0$ at $t=0$, the solution is

$$f_{cp} = \frac{Q}{\lambda_{cp}}[1 - \exp(-\lambda_{cp}t)], \qquad (A3)$$

where $Q = P\varepsilon(1-f_a)$. This equation can be inserted into Eq. (A2) in order to obtain the approximate time-dependent solution for f_{cp}. After rearranging, Eq. (A2) becomes

$$\frac{df_{cp}}{dt} = P\varepsilon(1-f_a)\exp(-\lambda_{cp}t); \qquad (A4)$$

substituting Eq. (A4) into Eq. (A1) and expanding gives

$$\frac{df_a}{dt} = P(1-f_a)[1 - \varepsilon + \varepsilon \exp \lambda_{cp}t] - \lambda f_a. \qquad (A5)$$

We define Z to be the term in the square brackets in Eq. (A5). Assuming that $\lambda/Z \approx \lambda/(1-\varepsilon) = \lambda'$ (this approximation should be valid over the temperature range investigated), then by using the initial condition that $f_a = 0$ at $t = 0$ the solution to Eq. (A5) is

$$f_a = \frac{P}{P+\lambda'}\left[1 - \exp\left[-(P+\lambda')\right.\right.$$
$$\left.\left.\times\left((1-\varepsilon)t + \frac{\varepsilon}{\lambda_{cp}}(1-e^{-\lambda_{cp}t})\right)\right]\right]. \qquad (A6)$$

Equation (A6) was used to plot the curves in Fig. 2 and to calculate the activation energies for the orthosilicates.

One important concern in the derivation of Eq. (A6) is the assumption of constant f_a used to obtain Eq. (A3). This assumption can be eliminated by modeling the close-pair (f_{cp}) and displacement-cascade (f_{dc}) contributions separately and summing their respective contributions to the total amorphous fraction (f_a):

$$\frac{df_{cp}}{dt} = P\varepsilon(1-f_a) - \lambda_{cp}f_{cp}, \qquad (A7)$$

$$\frac{df_{dc}}{dt} = P(1-\varepsilon)(1-f_a) - \lambda_{dc}f_{dc}. \qquad (A8)$$

An approximate solution for this set of equations can be obtained by assuming that the close-pair defect fraction achieves its steady state value much faster than the displacement-cascade defect fraction. This assumption is certainly valid at temperatures above the close-pair annealing stage (300 to 550 K for the orthosilicates in this study), whereas, it may or may not be valid at low temperatures. Solving for the steady-state solution for f_{cp} in Eq. (A7) and inserting this expression into Eq. (A8), the following expression is obtained:

$$\frac{df_{dc}}{dt} = P(1-\varepsilon)\left[1 - f_{dc} - \frac{\varepsilon P(1-f_{dc})}{\varepsilon P + \lambda_{cp}}\right] - \lambda_{dc}f_{dc}. \qquad (A9)$$

This equation can be rearranged to give

$$\frac{df_{dc}}{dt} + (S+\lambda_{dc})f_{dc} = S, \qquad (A10)$$

where

$$S = \frac{(1-\varepsilon)P\lambda_{cp}}{\varepsilon P + \lambda_{cp}}. \qquad (A11)$$

The linear homogeneous equation (A10) can be solved by standard methods. Using the boundary condition that $f_{dc} = 0$ at $t = 0$, the solution is

$$f_{dc} = \frac{S}{S + \lambda_{dc}} [1 - \exp - (S + \lambda_{dc})t]. \qquad (A12)$$

This equation can be inserted into Eq. (A7) in order to obtain an approximate time-dependent solution for f_{cp}. After rearranging, Eq. (A7) becomes

$$\frac{df_{cp}}{dt} + (\varepsilon P + \lambda_{cp})f_{cp} = \frac{\varepsilon P \lambda_{dc}}{S + \lambda_{dc}} + \frac{\varepsilon PS}{S + \lambda_{dc}} \exp - (S + \lambda_{dc}). \qquad (A13)$$

Using the initial condition that $f_{cp} = 0$ at $t = 0$, the solution for Eq. (A13) is given by

$$f_{cp} = \frac{\varepsilon P \lambda_{dc}}{(S + \lambda_{dc})(\varepsilon P + \lambda_{cp})} [1 - \exp - (\varepsilon P + \lambda_{cp})t]$$

$$+ \frac{\varepsilon PS \exp - (S + \lambda_{dc})t}{(S + \lambda_{dc})(\varepsilon P + \lambda_{cp} - S - \lambda_{dc})}$$

$$\times [1 - \exp - (\varepsilon P + \lambda_{cp} - S - \lambda_{dc})t]. \qquad (A14)$$

The total amorphous atom fraction is then given by the sum of Eqs. (A12) and (A14):

$$f_a = f_{dc} + f_{cp}. \qquad (A15)$$

Equation (A15) is difficult to apply to the experimental data, so Eq. (A6) was used to plot the lines in Fig. 2. The activation energies calculated from Eq. (A15) are the same as obtained from Eq. (A6), however, the slope of the line at the temperatures for stage I annealing is slightly modified.

[1] D. F. Mullica, W. O. Milligan, D. A. Grossie, G. W. Beall, and L. A. Boatner, Inorg. Chim. Acta **95**, 231 (1984).

[2] W. O. Milligan, D. F. Mullica, G. W. Beall, and L. A. Boatner, Acta Crystallogr., Sect. C: Cryst. Struct. Commun. **C39**, 23 (1983).

[3] M. Taylor and R. C. Ewing, Acta Crystallogr., Sect. B: Struct. Crystallogr. Cryst. Chem. **B34**, 1074 (1978).

[4] B. E. Burakov, E. B. Anderson, V. S. Rovsha, S. V. Ushakov, R. C. Ewing, W. Lutze, and W. J. Weber, in *Scientific Basis for Nuclear Waste Management XIX*, edited by W. M. Murphy and D. A. Knecht, MRS Symposia Proceedings No. 412 (Materials Research Society, Pittsburgh, 1996), p. 33.

[5] R. C. Ewing, W. J. Weber, and W. Lutze, in *Crystalline Ceramics: Waste Forms for the Disposal of Weapons Plutonium, NATO Workshop Proceedings*, edited by E. R. Merz and C. E. Walter (Academic Publishers, Dordrecht, The Netherlands, 1996), p. 65.

[6] R. C. Ewing, W. Lutze, and W. J. Weber, J. Mater. Res. **10**, 243 (1995).

[7] W. J. Weber, R. C. Ewing, and W. Lutze in *Scientific Basis for Nuclear Waste Management XIX*, edited by W. M. Murphy and D. A. Knecht, MRS Symposia Proceedings No. 412 (Materials Research Society, Pittsburgh, 1996), p. 25.

[8] L. T. Silver, in *Stable Isotope Geochemistry: A Tribute to Samuel Epstein*, edited by H. P. Taylor *et al.* (The Geochemical Society, Special Publication No. 3, Columbus, OH, 1991), p. 391.

[9] T. E. Krogh and G. L. Davis, Carnegie Inst. Wash. Publ. **74**, 619 (1975).

[10] L. Heaman and R. R. Parrish, in *Applications of Radiogenic Isotope Systems to Problems in Geology*, edited by L. Heaman and J. N. Ludden, MAC Short Course Volume 19 (Mineralogical Association of Canada, Toronto, 1991) p. 59.

[11] L. Babsail, N. Hamlin, and P. Townsend, Nucl. Instrum. Methods Phys. Res. B **59/60**, 1219 (1991).

[12] L. A. Boatner and B. C. Sales, in *Radioactive Waste Forms for the Future*, edited by W. Lutze and R. C. Ewing (Elsevier Science, Amsterdam, 1988), p. 495.

[13] R. R. Parrish, Can. J. Earth Sci. **27**, 1431 (1990).

[14] A. Lempicki, E. Berman, A. J. Wojtowicz, M. Balcerzyk, and L. A. Boatner, IEEE Trans. Nucl. Sci. **40**, 384 (1993).

[15] S. W. Allison, L. A. Boatner, and G. T. Gillies, Appl. Opt. **34**, 5624 (1995).

[16] A. Meldrum, L. A. Boatner, and R. C. Ewing, Phys. Rev. B **56**, 13 805 (1997).

[17] A. Meldrum, S. J. Zinkle, L. A. Boatner, and R. C. Ewing, Nature (London) **395**, 56 (1998).

[18] R. W. Reynolds, L. A. Boatner, C. B. Finch, A. Châtellain, and M. M. Abraham, J. Chem. Phys. **56**, 5607 (1972).

[19] A. Meldrum, L. A. Boatner, and R. C. Ewing, in *Microstructure Evolution During Irradiation*, edited by I. M. Robertson, G. S. Was, L. W. Hobbs, and T. Diaz de la Rubia, MRS Symposia Proceedings No. 439 (Materials Research Society, Pittsburgh, 1997), p. 697.

[20] A. Meldrum, L. A. Boatner, and R. C. Ewing, J. Mater. Res. **12**, 1816 (1997).

[21] L. M. Wang, Nucl. Instrum. Methods Phys. Res. B **141**, 312 (1998).

[22] W. J. Weber, R. C. Ewing, C. R. A. Catlow, T. Diaz de la Rubia, L. W. Hobbs, C. Kinoshita, Hj. Matzke, A. T. Motta, M. A. Nastasi, E. H. K. Salje, E. R. Vance, and S. J. Zinkle, J. Mater. Res. **13**, 1434 (1998).

[23] W. J. Weber, R. C. Ewing, and L. M. Wang, J. Mater. Res. **9**, 688 (1994).

[24] H. Abe, S. Yamamoto, and H. Naramoto, Nucl. Instrum. Methods Phys. Res. B **127/128**, 170 (1997).

[25] W. J. Weber and L. M. Wang, Nucl. Instrum. Methods Phys. Res. B **91**, 63 (1994).

[26] W. J. Weber, L. M. Wang, and N. Yu, Nucl. Instrum. Methods Phys. Res. B **116**, 322 (1996).

[27] W. J. Weber, J. Mater. Res. **5**, 2687 (1990).

[28] H. S. Virk, Radiat. Eff. Defects Solids **133**, 87 (1995).

[29] T. Tagami, A. Carter, and A. J. Hurford, Chem. Geol. **130**, 147 (1996).

[30] R. Yamada, T. Tagami, S. Nishimura, and H. Ito, Chem. Geol. **122**, 249 (1995).

[31] F. Dachille and R. Roy, J. Geol. **72**, 243 (1964).

[32] G. R. Lumpkin and B. C. Chakoumakos, Am. Mineral. **73**, 1405 (1988).

[33] A. Meldrum, L. M. Wang, and R. C. Ewing, Nucl. Instrum. Methods Phys. Res. B **116**, 220 (1996).

[34] L. M. Wang, M. Cameron, W. J. Weber, K. D. Crowley, and R. C. Ewing, in *Hydroxyapatite and Related Materials*, edited by P. W. Brown and B. Constantz (CRC Press, London, 1994), p. 243.

[35] R. C. Ewing, L. M. Wang, and W. J. Weber, in *Microstructure of Irradiated Materials*, edited by I. M. Robertson, L. E. Rehn, S. J. Zinkle, and W. J. Phythian, MRS Symposia Proceedings No. 373 (Materials Research Society, Pittsburgh, 1995), p. 347.

[36] K. L. Smith, N. J. Zaluzec, and G. R. Lumpkin, J. Nucl. Mater. **250**, 36 (1997).

[37] K. A. Jackson, J. Mater. Res. **3**, 1218 (1988).

[38] G. Carter and M. J. Nobes, J. Mater. Res. **6**, 2103 (1991).

[39] V. Heera, T. Henkel, R. Kögler, and W. Skorupa, Phys. Rev. B **52**, 15 776 (1995).

[40] F. Gao, D. J. Bacon, P. E. J. Flewitt, and T. A. Lewis, J. Nucl. Mater. **249**, 77 (1996).

[41] R. Webb and G. Carter, Radiat. Eff. **42**, 159 (1979).

[42] G. H. Kinchin and R. S. Pease, Rep. Prog. Phys. **18**, 1 (1955).

[43] M. L. Miller and R. C. Ewing, Ultramicroscopy **48**, 203 (1992).

[44] S. J. Zinkle and C. Kinoshita, J. Nucl. Mater. **251**, 200 (1997).

[45] H. M. Naguib and R. Kelly, Radiat. Eff. **25**, 1 (1975).

[46] L. M. Wang, W. L. Gong, and R. C. Ewing, in *Crystallization and Related Phenomena in Amorphous Materials*, edited by M. Libera, T. Haynes, P. Cebe, and J. Dickenson, Jr., MRS Symposia Proceedings No. 321 (Materials Research Society, Pittsburgh, 1994), p. 405.

[47] L. W. Hobbs, Nucl. Instrum. Methods Phys. Res. B **91**, 30 (1994).

[48] S. X. Wang, Ph.D. thesis, University of New Mexico, 1997.

[49] R. K. Eby, R. C. Ewing, and R. C. Birtcher, J. Mater. Res. **7**, 3080 (1992).

[50] E. H. Lee, P. J. Maziasz, and A. F. Rowcliffe, in *Phase Stability During Irradiation*, edited by J. R. Holland, L. K. Mansur, and D. I. Potter (TMS/AIME, New York, 1981), p. 191.

[51] P. P. Newcomer, J. C. Barbour, L. M. Wang, E. L. Venturini, J. F. Kwak, R. C. Ewing, M. L. Miller, and B. Morosin, Physica C **267**, 243 (1996).

[52] L. M. Wang, W. L. Gong, N. Bordes, R. C. Ewing, and Y. Fei, in *Microstructure of Irradiated Materials* (Ref. 35), p. 407.

[53] R. L. Fleischer, P. B. Price, and R. M. Walker, *Nuclear Tracks in Solids* (University of California Press, Berkeley, 1975).

[54] A. Miotello and R. Kelly, Nucl. Instrum. Methods Phys. Res. B **122**, 458 (1997).

[55] H. L. Heinisch and B. N. Singh, Philos. Mag. A **67**, 407 (1993).

[56] D. J. Bacon and T. Diaz de la Rubia, J. Nucl. Mater. **216**, 275 (1994).

[57] T. Diaz de la Rubia, R. S. Averback, and H. Hsieh, J. Mater. Res. **4**, 579 (1989).

[58] W. C. Butterman and W. R. Foster, Am. Mineral. **52**, 884 (1967).

[59] V. N. Parfenenkov, R. G. Grebenschikov, and N. A. Toropov, Dokl. Akad. Nauk SSSR **185**, 288 (1969).

[60] S. Lungu, J. Nucl. Mater. **19**, 157 (1966).

[61] M. Caro, A. Ardelea, and A. Caro, J. Mater. Res. **5**, 2652 (1990).

[62] I. Koponen, Phys. Rev. B **47**, 14 011 (1993).

[63] J. S. Kirkaldy and D. J. Young, *Diffusion in the Condensed State* (Institute of Metals, London, 1987).

[64] S. Ellsworth, A. Navrotsky, and R. C. Ewing, Phys. Chem. Miner. **21**, 140 (1994).

[65] M. Nastasi and J. W. Mayer, *Materials Science Reports* (North-Holland, Amsterdam, 1991), Vol. 6.